Journal of Cleaner Production 306 (2021) 127204

Contents lists available at ScienceDirect

Journal of Cleaner Production

journal homepage: www.elsevier.com/locate/jclepro

Synthesis of a novel three-dimensional porous carbon material and its highly selective Cr(VI) removal in wastewater

Hongxu Liang [a, b], Hongwei Zhang [a], Pinye Zhao [a], Xinkun Zhao [a], Haowei Sun [a], Zengchao Geng [a, b, *], Diao She [c, d, **]

[a] College of Natural Resources and Environment, Northwest A&F University, Yangling, 712100, China
[b] Key Laboratory of Plant Nutrition and the Agri-environment in Northwest China, Ministry of Agriculture, Yangling, 712100, China
[c] State Key Laboratory of Soil Erosion and Dryland Farming on the Loess Plateau, Northwest A&F University, Yangling, 712100, China
[d] Institute of Soil and Water Conservation, CAS&MWR, Yangling, 712100, China

ARTICLE INFO

Article history:
Received 2 November 2020
Received in revised form
17 January 2021
Accepted 18 April 2021
Available online 22 April 2021

Handling editor: Bin Chen

Keywords:
High performance
High selectivity
Wastewater treatment
Removal Cr(VI)
Adsorption

ABSTRACT

Cr(VI) in water severely affects human health. In this study, a kind of novel 3D porous carbon material (3D-PCM) was prepared using glucose and urea via two-stage-hydrothermal and activation method for Cr(VI) removal in wastewater. The SEM demonstrate that 3D-PCM has a developed pore structure, and BET test shows that its specific surface area reaches 1554.77 m^2/g. Batch adsorption experiments showed that the best pH is about 2.0 The Cr(VI) adsorption process on 3D-PCM follows pseudo-second-order kinetics and Freundlich model, and the maximum adsorption capacity reaches 837.19–951.65 mg/g (25–45 °C), which is higher than those of similar adsorbents in the world. Through the combination of chemical characterization and adsorption model analysis indicate that the main adsorption mechanisms on 3D-PCM include electrostatic interactions, ion complexation, physical adsorption, reduction and hydrogen bonding. Moreover, the multi-ion competitive simulation and adsorption and regeneration experiments showed that 3D-PCM has excellent selectivity and regenerative performance for Cr(VI) adsorption. Economic analysis shows that the manufacturing cost of 3D-PCM is low. Therefore, 3D-PCM is an effective and reusable material for Cr(VI) removal, and its preparation method is green and sustainable, which is expected to improve the problem of Cr(VI) pollution in water.

1. Introduction

The environmental problems caused by heavy metal emission in industry are very serious (Ramalingam et al., 2018). Chromium is one of the common heavy metals, primarily concentrated in electroplating, mining, leather and other industries produced in wastewater and domestic sewage (Kumar et al., 2015; Zehhaf et al., 2015; Kera et al., 2016). There are two main forms of chromium: Cr(VI) and Cr(III). Among them, Cr(III) is one of the trace elements in human body, which generally exists in sediment or adsorption state, which is difficult to migrate in the environment, and is easy to be converted into $Cr(OH)_3$ precipitation, resulting in less harm. (Ramalingam et al., 2018). In contrast, Cr(VI) is usually present in wastewater as oxygen anion due to the formation of oxygen anions, it is difficult to fix hexavalent chromium in clay minerals in the environment, so its fluidity is high. Moreover, Cr(VI) is present as an anionic oxide, it can enter the cell through an anionic channel easily accumulated in the human body and severely affects human health with a high carcinogenicity (Legrouri et al., 2017; Xu et al., 2019). The World Health Organization (WHO) stipulates that the maximum Cr(VI) content limit in surface water is 0.1 mg/L, and the allowable limit drinking water is 0.05 mg/L (Xu et al., 2019). The content of Cr(VI) in wastewater discharged from actual industry is 100 mg/L or even higher (Ballav et al., 2014). Therefore, it is urgent to treat industrial wastewater containing Cr(VI) to reduce its harm for humans after entering the environment.

Many methods have been tried to remove Cr(VI) in wastewater: adsorption, chemical precipitation, membrane filtration, electrochemical, catalytic reduction, and biological treatments (Pradhan

* Corresponding author. College of Natural Resources and Environment, Northwest A&F University, Yangling, 712100, China.
** Corresponding author. State Key Laboratory of Soil Erosion and Dryland Farming on the Loess Plateau, Northwest A&F University, Yangling, 712100, China.
E-mail addresses: gengzengchao@126.com (Z. Geng), diaoshe@ms.iswc.ac.cn (D. She).

https://doi.org/10.1016/j.jclepro.2021.127204
0959-6526/

et al., 2017; Yang et al., 2019; Zhu et al., 2019; Lv et al., 2019; Wang et al., 2020). Among them, the adsorption is based on the different adsorbents and can be used to remove a certain ion. Therefore, adsorption is widely used to eliminate pollution. The adsorbents currently used for Cr(VI) removal include carbon-based materials (Gu et al., 2013), biomass (Nameni et al., 2008), MOF (Li et al., 2017), oxide and agricultural residues (O'Connell et al., 2008). However, because Cr(VI) usually present in wastewater as oxygen anion, the adsorption capacity and selectivity of most adsorbents to Cr(VI) are low. Therefore, the synthetic of materials with a high performance and selectivity for Cr(VI) elimination has become one of the most pressing problems.

Carbon-based adsorbents are considered excellent materials for removing Cr(VI) because of their advantages of having a low cost, good adsorption capacity (Pakade et al., 2019). Among them, carbon spheres are considered to be an excellent material because of their high reactive activity. However, the specific surface area of carbon spheres is low, so that it is difficult to store pollutants and the adsorption ability of Cr(VI) is not high enough. Fortunately, the chemical activation treatment can increase specific surface area and surface defects, and improve the adsorption capacity of Cr(VI) by using activator to form pores in carbon spheres. Chromium anions can be electrostatically trapped by positively charged species, such as ammonium salts (Pan et al., 2019). Moreover, N in materials can release electrons to reduce Cr(VI), and the surface of the material can form defects to capture the Cr(VI) due to the incorporation of the N (Pakade et al., 2019). Therefore, the incorporation of N may improve the adsorption performance of an adsorbent for Cr(VI). During the different N doped, pyridinic-N and pyrrolic-N play a key role in the adsorption reaction. Our research showed that the N of secondary hydrothermal is almost pyridine-N and pyrrole-N compared with direct nitrogen doping N, which is very beneficial to removal of Cr(VI). Therefore, hydrothermal reaction again for N modification based on first step hydrothermal synthesis of highly active carbon spheres is a better method.

Synthesizing the above results, in this work, carbon spheres were synthesized via the hydrothermal reaction innovatively using inexpensive glucose as the raw material, and N elements were further mixed hydrothermal with urea to form N-modified carbon spheres (NM-CSs), then a KOH activation of NM-CSs synthesis novel 3D-PCM. Novel composite materials are currently one of the hot materials for metal ion removal, including conjugated composites (Awual., 2016; Awual., 2016a), organic-inorganic skeleton composites (Awual et al., 2019), optical composites (Awual et al., 2019) and immobilized surface composites (Awual., 2015, 2016b), etc. These materials are one of the competitive materials of 3D-PCM in the market. Compared with these new composite materials, 3D-PCM has the advantages of higher specific surface area, stronger selective adsorption performance and green and sustainable synthesis route, but the disadvantage is not as sensitive to metal ions as these composite materials (Awual., 2017; Awual et al., 2019b). Therefore, 3D-PCM is more suitable for the treatment of high-concentration industrial wastewater containing chromium.

In this study, the adsorption ability of 3D-PCM to Cr(VI) was investigated via a batch adsorption experiments. The structural properties of the materials and the adsorption mechanism were investigated using comprehensive physicochemical characterization technology and adsorption model calculations. The cost of 3D-PCM and its potential for large-scale application are analyzed economically.

2. Experiments and methods

Reagent information are in Text.S1 of the supporting information.

2.1. Preparation of NM-CSs

15 g of glucose and 0.375 g of sodium dodecyl sulfate (SDS) (glucose: SDS = 40:1) were put into a 250 ml hydrothermal reactor, and 150 ml of distilled water was added, then the rotational speed of 500 r/min and temperature of 185 °C were set, and the hydrothermal reaction last for 3 h. A mixture was collected by 220 nm filter paper, washed with 95% ethanol and deionized water, oven dried under 80 °C for 6 h, form the final carbon spheres (CSs).

3 g of carbon spheres and 3 g of urea (CSs: urea = 1:1) were put into 250 ml hydrothermal reactor, and 150 ml of distilled water was added, the following steps are consistent with the carbon spheres. The product was filtered by 220 nm filter membrane, washed with 95% ethanol and deionized water, oven dried under 80 °C for 4 h, to obtain carbon spheres (NM-CSs).

2.2. Preparation of 3D-PCM

The synthesized NM-CSs and KOH (NM-CSs:KOH = 1:3) were mixed, and ground for 5–10 min in a mortar, the mixture was transferred to a beaker with deionized water (ensure deionized water immersion material), and stirred on magnetic agitator for 24 h with rotational speed of 500–600 r/min. After stirring, dry moisture at 110 °C using a thermostatic blast dryer. The mixture was placed in a muffle furnace using Ar gas as a protective gas, activating under 800 °C for 2 h, and heating rate of 8 °C/min. The final product was filtered by 220 nm filter membrane after activation reaction, washed to neutral (pH = 7) with a large amount of deionized water, then washed with 95% ethanol for 3 times, oven dried under 80 °C for 4 h, to obtained 3D porous carbon materials (3D-PCM). The overall synthesis flow chart of 3D-PCM is shown in Fig. 1a.

2.3. Product characterization

The product was characterized via SEM-EDS mapping, TEM, the BET specific surface area, Raman spectroscopy, XRD, XPS, element analysis and the Zeta potential. The specific parameters are in Text S2 of the supporting information.

2.4. Batch adsorption experiment

Cr(VI) solution was configured with potassium dichromate in this study. The addition of 0.4 g/L adsorbent to a certain content of Cr(VI) solution, and the pH of the solution was adjusted using 0.01 mol/L NaOH and HCl. The adsorption process was performed in a constant temperature shock incubator. The Cr(VI) standard curve is shown in Fig. S1. The effects of pH (1.5–7), Cr(VI) concentration (40–800 mg/L), temperature (25–45 °C) and adsorption time (0.5–12 h) on the adsorption ability were tested. The calculation formula of the adsorption capacity (Eq. (1)) (Awual and Hasan., 2015):

$$q_e = \frac{(C_0 - C_1)V}{m} \quad (1)$$

where q_e (mg/g) is the after adsorption reaction reaches equilibrium, the adsorption capacity of Cr(VI), m (g) is the amount of 3D-PCM, C_0 (mg/L) is the initial content of Cr(VI), C_1 (mg/L) is the final content of Cr(VI), and V (L) is the solution volume.

2.5. Adsorption regeneration experiment

The detailed steps of the experiment are in Text S3 of the supporting information.

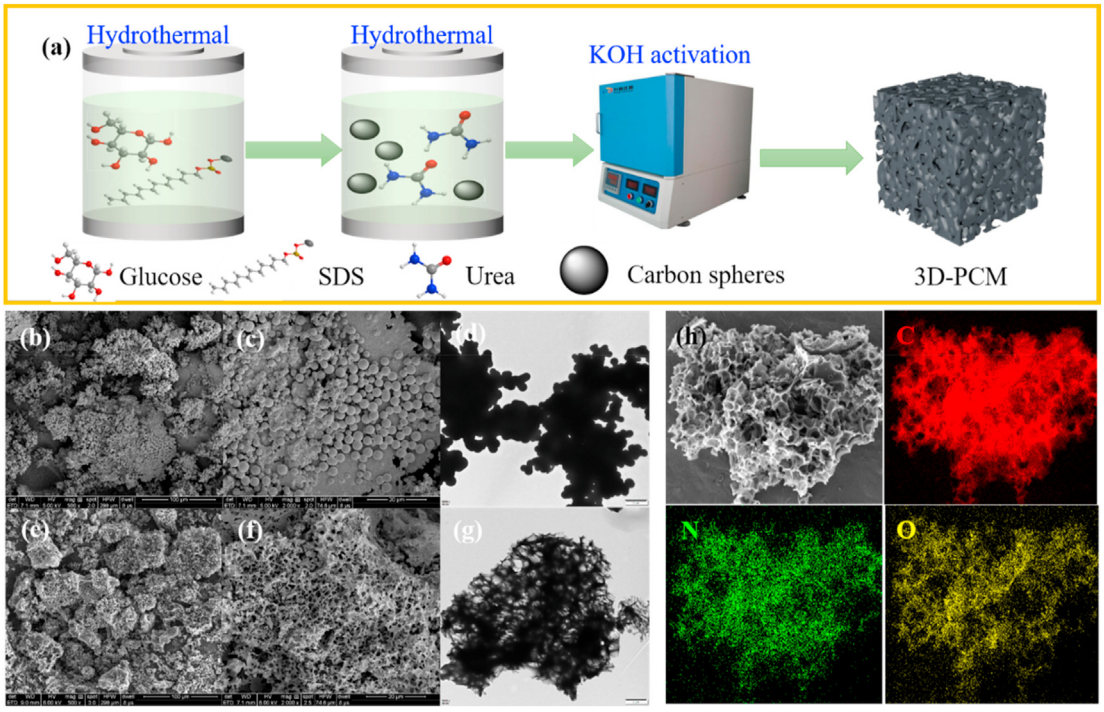

Fig. 1. 3D-PCM preparation flow chart and surface morphology diagram: a is preparation flow chart; b, c is SEM diagram of NM-CSs; d is TEM diagram of NM-CSs; e, f is SEM diagram of 3D-PCM; g is TEM diagram of 3D-PCM; h is SEM-mapping diagram of 3D-PCM.

3. Results and discussion

3.1. Characteristic description

The morphological properties of the NM-CSs and 3D-PCM are shown in Fig. 1b–h. SEM (Fig. 1a and b) shows that after N modification, the carbon sphere still maintains the spherical structure of the main body. TEM (Fig. 1c) shows that the modified carbon sphere is not hollow and that the porosity is very low. Through KOH activation, the NM-CSs were KOH etched to form 3D-PCM with a well-developed pore structure (Fig. 1e and f). This result is also confirmed via the TEM diagram (Fig. 1g) and specific surface area test (Table 1) of 3D-PCM. After KOH activation reaction, the specific surface area of 3D-PCM increased from 4.21 to 1554.77 m^2/g, which was very high, and the pore volume increased and pore size decreased, which increased the adsorption of nanopores (Table 1). The N_2 adsorption-desorption curves show that the 3D-PCM curve is of the I type, confirming that the adsorbent is primarily microporous (Fig. S2). This study further tested the 3D-PCM (Fig. 1h) using SEM-EDS mapping and found that the N elements were successfully modified in the material and the N and O groups were well distributed in the material, while the functional groups of the adsorbed Cr(VI) were primarily N and O groups. Therefore, the 3D-PCM adsorption sites were uniformly distributed. The surface structure of 3D-PCM is almost unchanged after adsorption reaction, while the EDS mapping shows that Cr(VI) is uniformly adsorbed on the material, which further confirms that the 3 adsorption sites are uniformly distributed (Fig. S3).

Raman spectroscopy can characterize the basic properties of adsorbent (Liu et al., 2015). The NM-CSs and 3D-PCM were so tested in this study (Fig. 2a). The D-band and G-band characteristic peaks of carbon materials were found in both materials. Among them, the D-band is about 1340 cm^{-1} and the G-band is about 1580 cm^{-1} (Sun and Li, 2004). Among these peaks, D-band indicates lattice defects in the material, a G-band indicates in-plane stretching vibrations sp^2 the hybridization of C atoms (Xu et al., 2018). The G-band peak of the NM-CSs is substantially higher than that of the D-band, which indicates that the lattice degree is high. The D-band and G-band peak intensities of 3D-PCM were basically equal ($I_D \approx I_G$), indicating that 3D-PCM belonged to amorphous carbon, and there was more amorphous carbon in internal disorder. This result may be attributable to the incorporation of N elements and the KOH activation reaction. The study found N can increase the structural defects of the material lattice, while KOH etching destroys a part of the lattice structure; thus, the D-band peak of 3D-PCM clearly increases (Wang et al., 2018). This study used XRD to test the crystallinity of NM-CSs and 3D-PCM (Fig. 2b), The results show that the XRD diffraction curves and diffraction peaks of NM-CSs and 3D-PCM coexist, confirming the presence of lattice and amorphous lattice structures in the material (Liang et al., 2020). NM-CSs and 3D-PCM presented a wide diffraction peak near $2\theta = 24°$, which was formed by interlayer stacking of the graphite phase. Combined with JCPDS 75–1621, $2\theta = 24°$ belongs to the (002) surface of graphitic, indicating that NM-CSs and 3D-PCM belong to a graphite phase structure, similar to that of graphitic carbon (Yuan et al., 2008).

Table 1
BET specific surface area and pore size distribution.

Name	BET surface area (m^2/g)	Average pore size (nm)	Total pore volume (cm^3/g)
NM-CSs	4.21	13.65	0.01
3D-PCM	1554.77	1.78	0.69

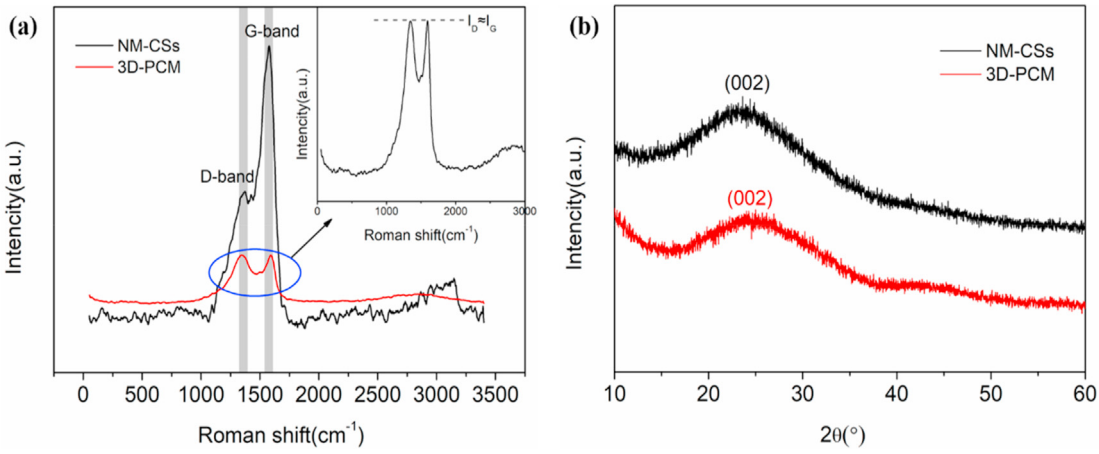

Fig. 2. Raman Spectra and XRD diagram of NM-CSs and 3D-PCM: a is Raman Spectra diagram; b is XRD diagram.

In this work, to explore the elemental content and chemical structure of the adsorbent, an XPS analysis and elemental analysis of NM-CSs and 3D-PCM were performed. Elemental analysis found that the N element was successfully modified into the material (Table 2), which that proves Fig. 1h result. Because sodium dodecyl sulfate is involved in the synthesis process of the material, S elements also exist in the material. After activation treatment, the content of O element in the material decreased slightly, which because of the reduce of oxygen groups by KOH high temperature etching. The XPS test found that the C 1s, O 1s and N 1s peaks existed in the adsorbent (Fig. 3). In C 1s peak, existence of two C-groups, the characteristic peak at 286.4 eV represents the C—C, C═C and CH_x, and at 287.1 eV represents the C—N and C—OH; in O 1s peak, existence of two O-groups, the characteristic peak at 531.7 eV represents the C═O and at 533.0 eV represents the -C-O-; in N 1s peak, there are three N-groups, the characteristic peak at 399.0 eV represents the pyridinic-N, a at 400.3 eV represents the pyrrolic-N, and at 406.1 eV represents the oxidic-N (Okpalugo et al., 2005). The emergence of N 1s peaks further confirms the conclusion drawn from Fig. 1h and Table 2 that N elements can be effectively incorporated by hydrothermal treatment. Studies have found that N functional groups play a highly important role in adsorption of Cr(VI), and pyrrole N is particularly effective (Ko et al., 2018). The XPS results confirmed the presence of more oxygen-containing functional groups as well as pyridinic-N and pyrrolic-N in 3D-PCM, which indicates that 3D-PCM has an good ability for removal of Cr(VI), which can effectively reduce the harm of Cr(VI) in the environment.

3.2. Adsorption studies

3.2.1. Effect of the pH, Cr(VI) content and temperature on adsorption

The pH value of the adsorption solution has a great influence on the adsorption reaction because under different pH conditions, the existence of ions will change (Awual et al., 2016; Awual, 2019). When the pH < 2, Cr(VI) mainly as H_2CrO_4; when the 2<pH < 6.8, Cr(VI) mainly as $HCrO_4^-$ and $Cr_2O_7^{2-}$; when the pH > 6.8, Cr(VI) mainly as CrO_4^{2-} (Wu et al., 2013). Moreover, the pH affects the Zeta potential of the adsorbent surface and changes the electrical properties of the 3D-PCM. Therefore, the adsorption process of Cr(VI) on 3D-PCM under different pH conditions must be studied. The Zeta potential of 3D-PCM under different pH (2—6) conditions was tested. The results showed that (Fig. 4a) the zero charge point (pH_{pzc}) of 3D-PCM was approximately 2.5, and when pH > 2.5, the surface of 3D-PCM was negatively charged, this time with Cr(VI), to produce a like charge repulsive effect; when pH < 2.5, the 3D-PCM surface was positively charged, and there was electrostatic adsorption on Cr(VI). In this work, content of Cr(VI) as 100 mg/L, the pH was 2, and the NM-CSs and 3D-PCM usage as 0.4 g/L were set. The adsorption properties of Cr(VI) on 3D-PCM were tested under different pH (1.5—7) conditions. The adsorption capacity of Cr(VI) by NM-CSs was significantly lower than that by 3D-PCM. Therefore, KOH activation treatment was necessary and effective for the adsorption reaction (Fig. 4b). As shown in Fig. 4b, the best adsorption pH is near 2, and as the pH increases, the adsorption performance gradually decreases, which corresponds to the results of the zeta potential test. When pH < 2, 3D-PCM adsorption capacity of Cr(VI) will decrease, because at this point, Cr(VI) mainly exists as H_2CrO_4, which cannot produce electrostatic adsorption. Interestingly, the actual chromium containing wastewater is generally acidic, which is very favorable for 3D-PCM adsorption of Cr(VI) reaction.

The higher the content of Cr(VI) is, the greater the content difference between adsorbent and solution will be, and the potential energy of solvent produced by a concentration difference will push Cr(VI) near the adsorbent, which will affect the adsorption reaction (Liang et al., 2020). In addition, the adsorption time is also an important factor affecting the adsorption process (Awual et al., 2019c). The Cr(VI) content to 40—400 mg/L, the adsorbent usage to 0.4 g/L, the pH was 2, and the change in 3D-PCM ability in 0.5—12 h was investigated. The results show that (Fig. 4c) with the increase Cr(VI) content, the adsorption ability of Cr(VI) also increases, which agrees with the conclusion that the concentration difference drives Cr(VI) to the adsorbate and the contact rate between adsorbent and Cr(VI) increases. The 3D-PCM removal rate of Cr(VI) was over 99.99% in the range of 40—100 mg/L (0.4 g/L of adsorbent), and the solution changed from orange to clear and transparent (Fig. 4e). When the Cr (VI) content is higher than 200 mg/L, 3D-PCM removal rate of Cr (VI) begins to decrease, which is because the limited amount of adsorbent used was not sufficient to completely remove Cr(VI). Therefore, in practical applications, when the Cr(VI) content is below 100 mg/L, 3D-PCM usage can be

Table 2
Element analysis table.

Name	C (%)	H (%)	O (%)	N (%)	S (%)
NM-CSs	61.61	1.225	32.946	3.58	0.133
3D-PCM	60.43	1.369	30.053	0.66	0.160

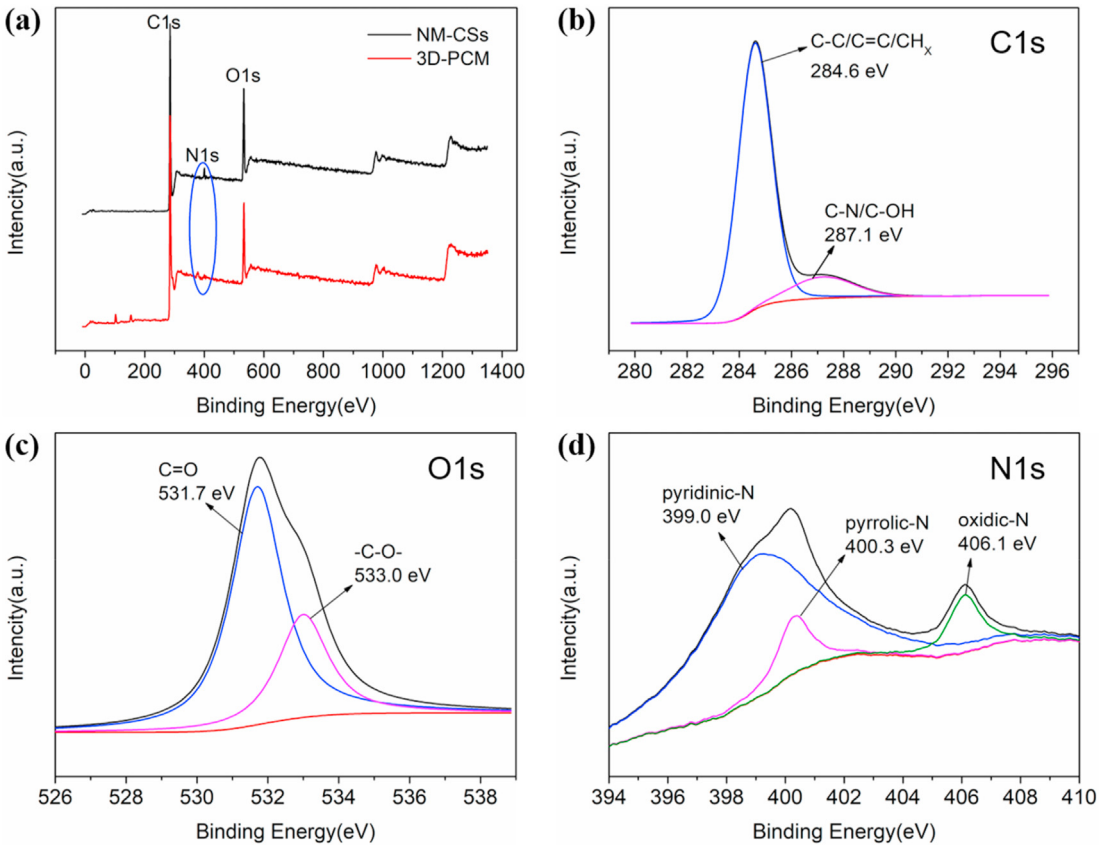

Fig. 3. XPS diagram: a is XPS diagram of NM-CSs and 3D-PCM; b is C1s diagram of 3D-PCM; c is O1s diagram of 3D-PCM; d is N1s diagram of 3D-PCM.

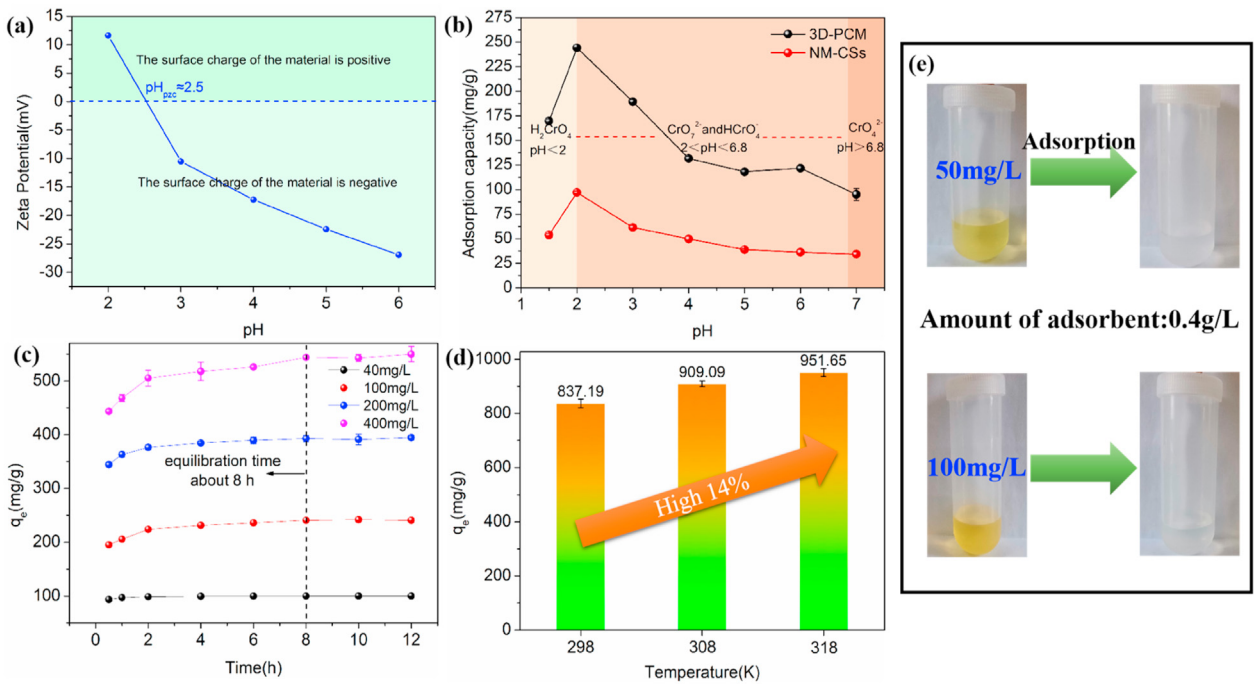

Fig. 4. Influence factor of adsorption: (a) pH; (b) Cr(VI) concentrations; (c) Zeta potential; (d) Temperature; (e) is actual adsorption effects.

set to 0.4 g/L. When the Cr(VI) content exceeds 200 mg/L, the adsorbent dose must be increased to ensure the removal effect.

The 3D-PCM adsorption of Cr(VI) is in keeping with the laws of thermodynamics, and temperature has a certain effect on adsorption. The concentration of Cr(VI) was set as 800 mg/L, the dosage of 3D-PCM was 0.4 g/L, the adsorption time was 24 h, and the pH was

2, the adsorption ability of 3D-PCM to Cr(VI) below 25–45 °C was investigated. The results found that (Fig. 4d) with the increase in temperature, the adsorption ability increased by approximately 14% from 837.19 mg/g to 951.65 mg/g, which proved that the increase in temperature benefited the adsorption, due perhaps to the increase in the molecular motion rate and contact probability with adsorbent. The temperature is generally above room temperature (25 °C) in an actual wastewater treatment plant, which benefits the higher effect of 3D-PCM.

Based on the results of different pH, Cr(VI) initial concentration and temperature effects on the adsorption process and performance, this study found that the optimal removal conditions for the treatment of chromium containing wastewater using 3D-PCM in real life are as follows: adsorption pH = 2 and adsorption temperature 45 °C.When the Cr(VI) content is below 100 mg/L, 3D-PCM usage can be set to 0.4 g/L, when the Cr(VI) content exceeds 200 mg/L, the adsorbent dose must be increased to ensure the removal effect.

3.2.2. Kinetic model

In this work, the solution pH = 2, the temperature to 25 °C, the adsorbent usage to 0.4 g/L, the Cr(VI) content to 40 mg/L and the adsorption ability was tested at 30–1440 min. The data was treated with pseudo-first-order kinetic model (Eq. (2)), pseudo-second-order kinetic model (Eq. (3)) and general order kinetic model (Eq. (4)) fitting (Lima et al., 2015).

$$q_t = q_e[1 - \exp(-k_1 t)] \tag{2}$$

$$q_t = \frac{q_e^2 k_2 t}{(1 + q_e k_2 t)} \tag{3}$$

$$q_t = q_e - \frac{q_e}{\left[k_N (q_e)^{n-1} t(n-1) + 1\right]^{\frac{1}{n-1}}} \tag{4}$$

where q_t is the adsorption capacity of Cr(VI) on 3D-PCM at time t; k_1 and k_2 is the model rate constant; n is the order of the kinetics; and k_N is the N order rate constant.

The kinetic fitting results found that (Fig. 5a, b, c and Table 3), the pseudo-second-order kinetic and general order kinetic model R^2 values were 0.9999, which higher than that of the pseudo-first-order kinetic model (R^2 = 0.9993). Moreover, the pseudo-second-order kinetic and general order kinetic model projected q_e values are 100.27 mg/g and 100.11 mg/g, respectively, closer to the actual q_e values (100 mg/g), therefore, the pseudo-second-order and general order kinetic model are suitable for explaining the adsorption reaction of Cr(VI) on 3D-PCM.

According to general order kinetic, in an adsorption reaction, the order of the adsorption should be consistent with the order of chemical reaction (Lima et al., 2015). The n value of Eq. (4) is calculated to be 1.85, which proves that the order of adsorption kinetics is very close to that of the pseudo-second-order kinetic, which showed that the 3D-PCM adsorption of Cr(VI) is a dominated by chemical adsorption, and physical and chemical adsorption coexist (Ho et al., 2000).

3.2.3. Diffusion model of adsorption

To further explore the control steps of the Cr(VI) adsorption reaction on 3D-PCM on the basis of kinetics, this study fitted and analyzed the intraparticle diffusion model (Eq. (5)). The Cr(VI) content to 40–400 mg/L, the adsorbent usage to 0.4 g/L, the pH was 2, and the change of adsorption performance within 0–12 h was tested.

$$q_t = K_{id} t^{0.5} + C \tag{5}$$

where C is the model constant; and K_{id} (mg/g·min$^{0.5}$) is the model diffusion rate constant.

The fitting results (Fig. 5d and Table 4) of the model are indicate that the 3D-PCM adsorption of Cr(VI) is divided into three stages, and the equation parameters of model fitting show that the model without going through zero point, which indicating that the adsorption reaction controlled by multiple factors, mainly membrane diffusion and intraparticle diffusion (Liang et al., 2019, 2020). The first stage is 0–120 min, this stage is the surface diffusion stage: the adsorbent has begun to adsorb pollutants, the adsorption sites are not occupied by pollutants, a content difference exists between Cr(VI) solution and adsorbent, and the resulting solvent potential energy drives Cr(VI) to the adsorbent; thus, the adsorption rate is faster. Moreover, with the increase in Cr(VI) content, the content difference increases and the adsorption rate increases. The value of $K_{id,1}$ from the slope of the curve verifies this conclusion (Table 4), at this stage, membrane diffusion plays a key role. The period of 120–480 min is the second stage of adsorption, when the adsorption sites on the adsorbent are gradually occupied by Cr(VI). With increase adsorption time, the difference between the Cr(VI) on the 3D-PCM and the Cr(VI) in the solution becomes progressively smaller, and even the Cr(VI) content on the 3D-PCM is higher than the Cr(VI) content in the solution. Therefore, the adsorption rate will weaken and $K_{id,2}$ is less than $K_{id,1}$ (Table 4). In this stage, membrane diffusion and intraparticle diffusion synergistically control the adsorption process of Cr(VI) on 3D-PCM. After 480 min, the adsorption process enters the final stage, this phase will achieve final adsorption equilibrium. The adsorption rate of the adsorbent in this stage is equal to the desorption rate. With the extension of time, the adsorption will change again only slightly, and the adsorption will reach equilibrium.

In order to understand the control factors and adsorption mechanism of adsorption reaction, the Boyd diffusion model (Eq. (6)(7) (8)) is used to fit the test data, and the results are discussed in combination with the above model (Ketelle and Boyd, 1947).

$$F = 1 - \left(\frac{\pi^2}{6}\right) exp(-B_t) \tag{6}$$

$$F = \frac{q_t}{q_e} \tag{7}$$

$$B_t = -0.4977 - ln(1 - F) \tag{8}$$

where B_t is the correlation function of F; and F is the ratio of adsorption capacity at t time to equilibrium adsorption capacity.

Fig. 6 showed the fitting lines of the Boyd model to the test data. The Boyd model fits the adsorption reaction of 40–400 mg/L Cr(VI) concentrations well, confirming that it is suitable for the interpretation 3D-PCM adsorption Cr(VI). The straight line fitted by the model is extended without passing through zero point, which indicates that the adsorption reaction is controlled by multiple factors. This conclusion confirms the results of the pseudo-second-order kinetic and the intraparticle diffusion model. Therefore, the adsorption process of Cr(VI) on 3D-PCM mainly chemical adsorption, and physical adsorption is also involved, process is controlled by multiple factors.

3.2.4. Equilibrium isotherms

Adsorption equilibrium isotherms can indicate the distribution of adsorb on the surface of liquid and adsorbent, and also be used to

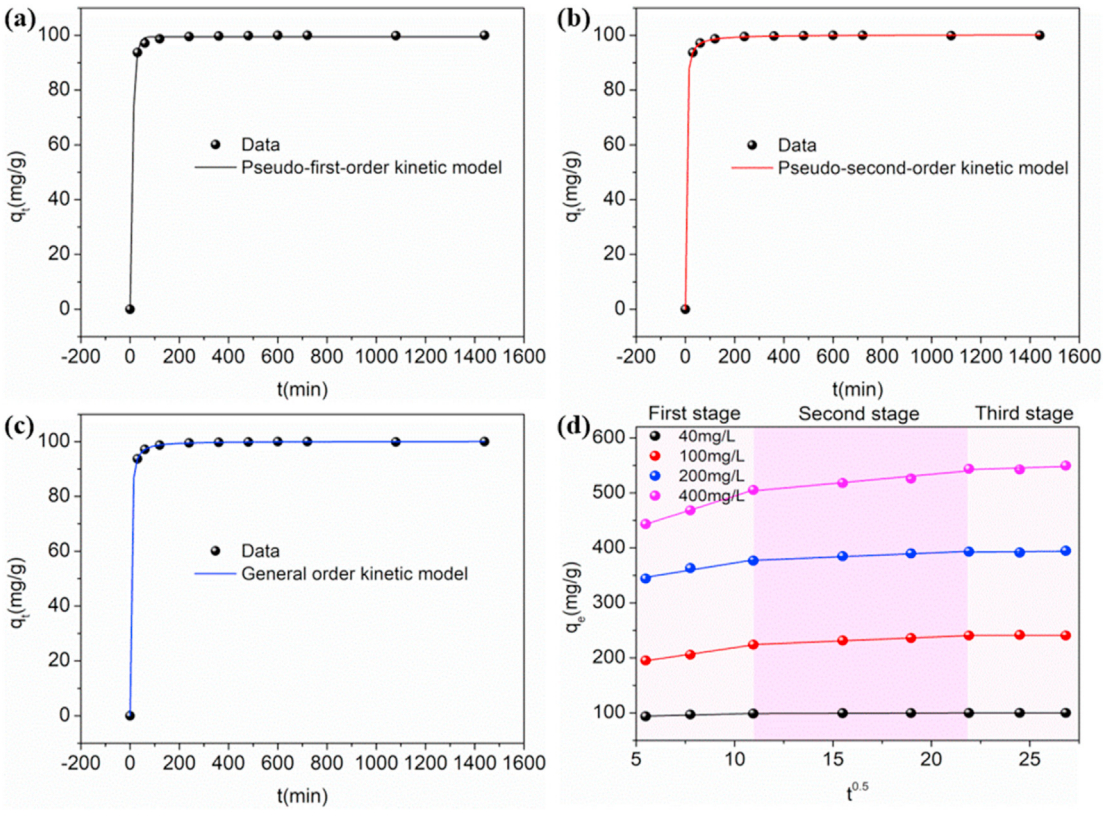

Fig. 5. Adsorption kinetics model and intraparticle diffusion model: a, b, c is adsorption kinetics model; d is intraparticle diffusion model.

Table 3
Adsorption Kinetic parameters.

Model name	Model related parameters
Pseudo-first-order	$k_1 = 9.36 \times 10^{-2}$, $q_e = 99.48$, $R^2 = 0.9993$
Pseudo-second-order	$k_2 = 4.86 \times 10^{-3}$, $q_e = 100.27$, $R^2 = 0.9999$
General order	$k_N = 7.23 \times 10^{-3}$, $q_e = 100.11$, $n = 1.85$, $R^2 = 0.9999$

understand the relationship between the content of adsorbate and the accumulation of adsorbate on the surface of adsorbent at constant temperature, which is of great significance to the design of materials in wastewater treatment (Awual., 2017). For a solution pH = 2, temperature of 25 °C, adsorbent amount of 0.4 g/L, and Cr(VI) content of 40–800 mg/L, the adsorption capacity of adsorbent at of 298, 308, and 318 K was measured. The experimental data were evaluated using Langmuir (Eq. (9)) and Freundlich (Eq. (10)) models in this study.

$$q_e = \frac{K_L q_{max} c_e}{1 + K_L c_e} \tag{9}$$

$$q_e = K_F c_e^{\frac{1}{n}} \tag{10}$$

where K_L, K_F and n is the model constant.

The results of the isotherm are showed that the compare with Langmuir model, Freundlich model has higher R^2 value (Table 5), and the trend of the curve in Fig. 7 tends to the Freundlich model, indicating that the Freundlich isotherms is suitable for the adsorption reaction of Cr(VI) on 3D-PCM. Generally, the fitting of the Freundlich model indicates that the adsorbent is a multimolecular layer, which also agrees with the three-dimensional characteristics of the adsorbent. The n value is more critical in the Freundlich model, which can show the difficulty of the adsorption process, the larger the n value, the easier the adsorption. In the isotherm calculation parameter table (Table 5), the n value of the three temperature conditions is greater than 1, which shows that the adsorption of Cr(VI) on 3D-PCMis favorable adsorption, and the 1/n value is less than 0.5, which shows that the adsorption reaction occurs easily (Liang et al., 2020). In Freundlich model, the K_F value represents the ability of the adsorbent, the larger the K_F, the higher the adsorption ability, K_F is greater than 160 for 3D-PCM, which confirms the excellent adsorption performance of 3D-PCM to Cr(VI). As the temperature increases, the adsorption capacity at each point on the isotherm increases accordingly, indicating that an increase in temperature promotes the adsorption reaction, which is consistent with Fig. 4d conclusion.

Table 4
Parameters of intraparticle diffusion model for 3D-PCM adsorption.

Initial concentration of Cr (VI) (mg/g)	$K_{id,1}$ (mg/g·min$^{0.5}$)	C_1	R^2	$K_{id,2}$ (mg/g·min$^{0.5}$)	C_2	R^2
40	0.88	89.40	0.8170	0.11	97.65	0.8639
100	5.27	165.92	0.9932	1.50	207.79	0.9966
200	5.81	314.52	0.9211	1.51	360.73	0.9852
300	11.35	380.83	0.9994	3.34	467.07	0.9307

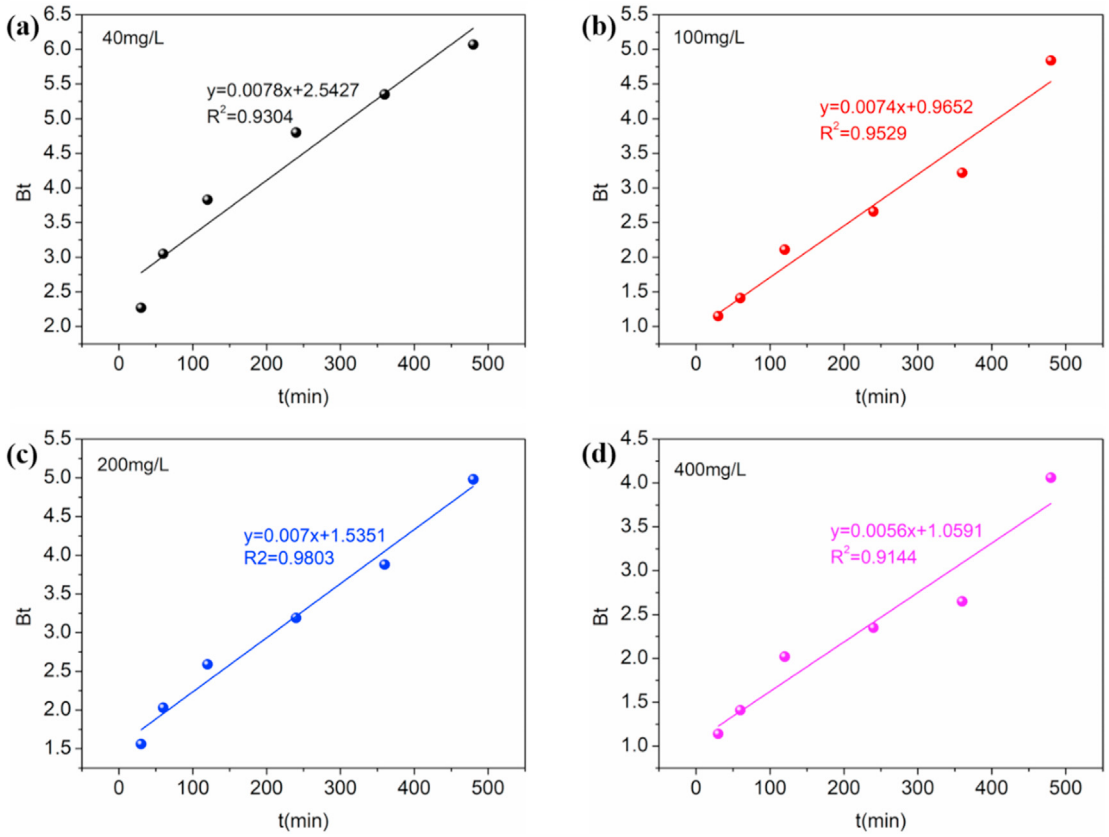

Fig. 6. Linear fitting Diagram between B_t and t: (a)40 mg/L; (b)100 mg/L; (c)200 mg/L; (d)400 mg/L.

Table 5
Parameters of isothermal adsorption model.

Model		298K	308K	318K
	$q_{max,exp}$ (mg/g)	837.19	909.09	951.65
Langmuir model	q_{max} (mg/g)	862.59	928.83	962.99
	K_L (L/mg)	0.0180	0.0179	0.0201
	R^2	0.8280	0.8481	0.8652
Freundlich model	K_F (mg/g/(mg/L)$^{1/n}$)	164.50	166.26	178.52
	n	3.89	3.72	3.75
	R^2	0.9728	0.9746	0.9784

3.2.5. Thermodynamics calculations of adsorption

To further explore the thermodynamic changes and adsorption mechanisms of the adsorption process, based on the isotherm model, the changes in free energy (ΔG°), heat (ΔH°) and entropy (ΔS°) were calculated. The thermodynamic formulas:

$$K_a = \frac{1000 K_L M_{adsorbate} C_{adsorbate}}{\gamma} \quad (11)$$

$$\Delta G^\circ = -RTlnK_a \quad (12)$$

$$\Delta G^\circ = \Delta H^\circ - T\Delta S^\circ \quad (13)$$

$$lnK_a = \frac{\Delta S^\circ}{R} - \frac{\Delta H^\circ}{RT} \quad (14)$$

where R (8.314 J/(mol·K)) is the universal gas constant, and T (K) is the temperature.

The Langmuir constants (K_L) were transformed dimensionless (K_a) using the method published by Lima et al. (Lima et al., 2019, 2019). Based on Eq. (11)–(14) calculation, it is found that $\Delta G^\circ<0$, and as the temperature increases, the absolute value of the ΔG° increases, confirming that the adsorption reaction of Cr(VI) on 3D-PCM is spontaneous reaction (Table 6), and the higher the temperature, the easier Cr (VI) is to be 3D-PCM adsorbed, which supports the conclusion drawn from Fig. 4d and the Freundlich models (Liang et al., 2019). A temperature increase promotes the adsorption process.

The ΔH° and ΔS° are calculated by plotting $\ln K_a$ against $1/T$ and fitting the intercept and slope of the straight line (Xu et al., 2019). $\Delta H^\circ>0$ indicates that the adsorption is endothermic, that is, an increase in temperature promote to adsorption reaction, which is consistent with the above results. $\Delta S^\circ>0$ indicates that the degree of disorder of the adsorbed solution increases, which is attributed to the acceleration of molecular motion and water replacement caused by the absorption of heat (Bhaumik et al., 2016; Xu et al., 2019).

3.3. Competing ion simulation in wastewater

Generally, in wastewater containing Cr(VI), there are many competing ions. Therefore, for the experiment, set the Cr(VI) content at 100 mg/L, add 50 mg/L (general conditions) or 200 mg/L (limiting conditions, and the concentration of other ions is twofold that of Cr(VI)) of Ca^{2+}, SO_4^{2-}, PO_4^{3-}, CO_3^{2-}, Mn^{7+}, Zn^{2+}, Cd^{2+} and Pb^{2+} to explore the selective adsorption of Cr(VI) on 3D-PCM.

The multi-ion competition simulation indicated that 3D-PCM had an excellent selective adsorption on Cr(VI), SO_4^{2-}, Mn^{7+}(MnO_4^-) and PO_4^{3-} had a slight effect on 3D-PCM adsorption of Cr(VI), and the other ions had an even slighter effect on 3D-PCM adsorption of

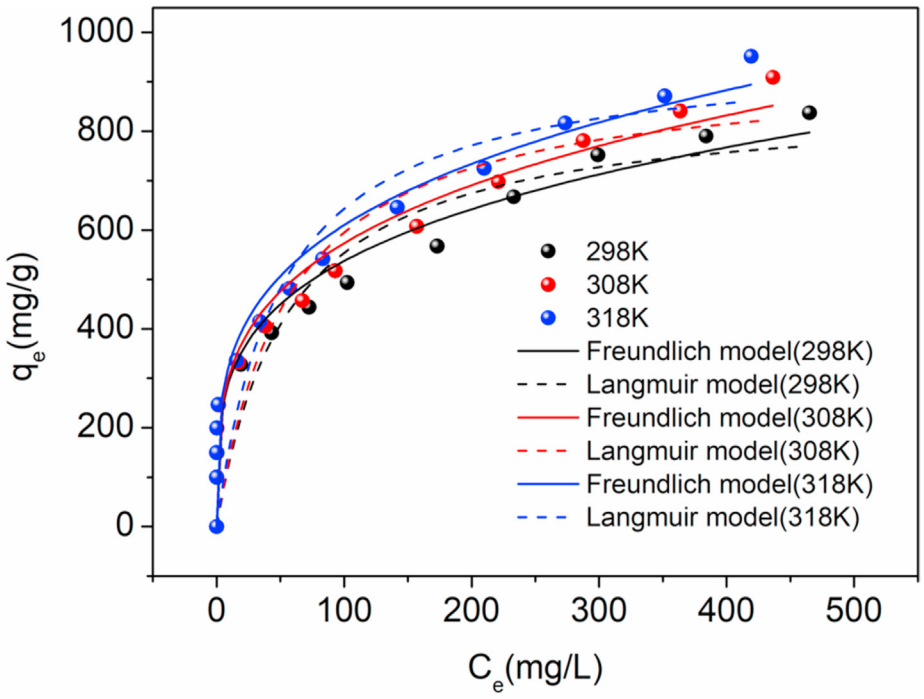

Fig. 7. Adsorption isotherm model.

Table 6
Thermodynamic parameters for the adsorption of 3D-PCM.

T(K)	K_a (L/mol)	ΔG°(kJ/mol)	ΔH°(kJ/mol)	ΔS°(kJ/(K/mol))
298	9.359×10^2	−16.96	42.48	0.224
308	9.307×10^2	−17.52		
318	1.045×10^3	−18.41		

Cr(VI), which was owing to the presence of Cr(VI) as oxygen anions in water in a form similar to that of SO_4^{2-}, $Mn^{7+}(MnO_4^-)$ and PO_4^{3-} (Fig. 8) (Zhitkovich, 2005). With Ca^{2+}, SO_4^{2-}, PO_4^{3-}, CO_3^{2-}, Mn^{7+}, Zn^{2+}, Cd^{2+}, Pb^{2+} and Cr(VI) in the nine-ion competition simulation, when the competitive ion content was 50 mg/L, the 3D-PCM adsorption ability decreased by only 10.11%; when the competitive ion content was 200 mg/L, the 3D-PCM adsorption ability decreased by only 15.44%. Under the extremely competitive condition in which the competitive ion content was twice the Cr(VI) concentration, the 3D-PCM adsorption ability to Cr(VI) remained above 84%. 3D-PCM has an excellent selective adsorption for Cr(VI), and can be applied to a variety of wastewater containing chromium to reduce the harm caused by Cr(VI) discharge to the water and soil environment.

3.4. Adsorption regeneration

Regeneration performance of materials is one of the important factors in industrial application (Awual, 2019). In this work, seven times adsorption-desorption regeneration experiment showed that the adsorption ability of Cr(VI) decreased rapidly in the first four adsorption cycles (Fig. 9). After the fourth cycle, the adsorption capacity stabilized at approximately 87.58% of the initial adsorption. This result shows that 3D-PCM has an good regeneration adsorption performance for Cr(VI), which can be used for many times in the actual treatment of wastewater containing chromium to achieve the purpose of sustainable clean production. To explore the reasons for the decrease in adsorption capacity, 3D-PCM after 3 adsorption-desorption cycles morphology and elemental composition were characterized using SEM and elemental analysis. The results showed that the surface morphology was largely unchanged after cyclic adsorption, indicating that the physical adsorption was

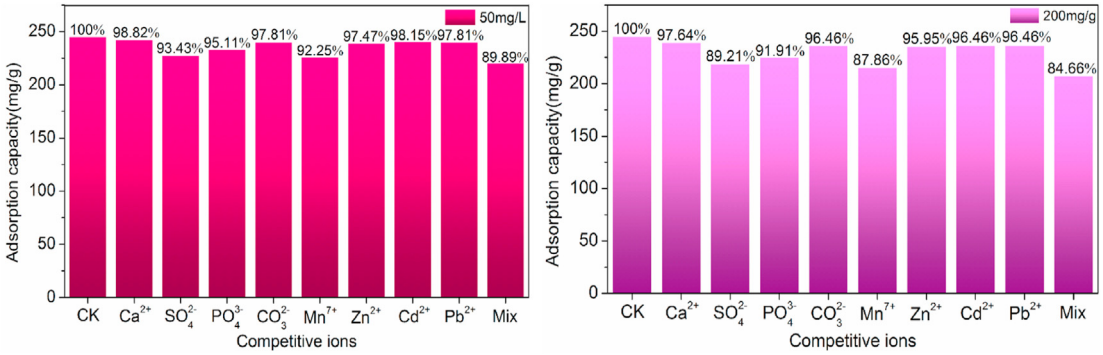

Fig. 8. Competitive ion simulation.

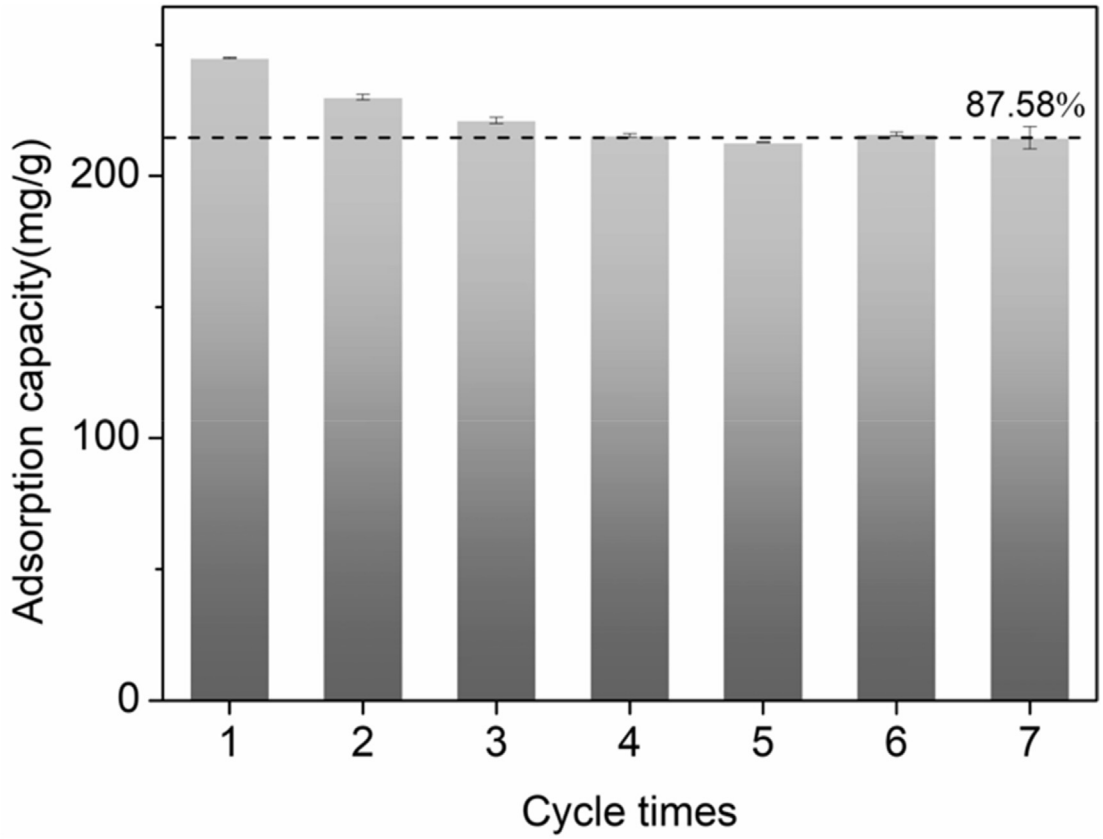

Fig. 9. Adsorption-desorption cycle experiment.

not affected. O and N elements decreased significantly (Fig. S4 and Table S1), which may be the main cause of the decrease in adsorption capacity. NaOH destroyed N and O groups such as −OH and $-NH_3^+$, thereby weakening the adsorption.

3.5. Economic analysis

In order to explore the possibility of 3D-PCM becoming a large-scale adsorbent production, it is necessary to calculate the cost and other factors. The synthesis process of 3D-PCM requires glucose, SDS, KOH and urea. In China, 1 t of glucose is about 464.86 $, 1 t of SDS is about 1549.52 $, 1 t of KOH is about 1007.19 $, and 1 t of urea is about 263.42 $. Based on this price, the raw material cost of 1 g 3D-PCM was calculated in this study, and the calculation results are shown in Table 7. The raw material cost of 1 g of 3D-PCM is about 0.026 $. Compared with other chromium adsorbents, the preparation cost of 3D-PCM is lower. Moreover, the synthesis process of 3D-PCM is green and sustainable, without the use of dangerous reagents, and the adsorbent is not doped with precious metals, which reduces the risk of secondary pollution after 3D-PCM enters the environment and is in line with the concept of cleaner production. Combined with the high adsorption performance and low cost, 3D-PCM has the potential to large-scale production and is expected to reduce the harm of Cr(VI) pollution in the environment.

Table 7
Price list of raw materials needed to synthesize 1g 3D-PCM.

Raw material	Weight (g)	Price (¥)	Price ($)
Glucose	30	0.09	0.0139
SDS	0.75	0.0075	0.0011
Urea	3	0.0051	0.0009
KOH	9	0.0585	0.0091
Total	42.75	0.1681	0.0260

3.6. Adsorption mechanism

The results of the kinetic and adsorption diffusion model showed that the adsorption reaction of Cr(VI) on 3D-PCM is mainly chemisorption, and there is physical adsorption (sections 3.2 and 3.3). The elemental mapping of 3D-PCM after adsorption Cr(VI) was performed using the SEM-EDS mapping. It was found that the distribution of Cr, O, and N on 3D-PCM was similar, confirming that Cr(VI) was closely related to the N and O groups (Fig. S3) (Ding et al., 2020). Moreover, EDS analysis found that Cr was mainly Cr(VI) in 3D-PCM, but there was also a small amount of Cr(III), which confirmed that 3D-PCM had a certain reduction effect on Cr(VI) (Fig. S4). The Zeta potential indicates (Fig. 4a) that when the pH < 2.5, the surface electrical properties of the 3D-PCM is positive, and the N is mainly present as NH_3^+ through the electrostatic interaction adsorption of Cr(VI); when pH > 2.5, the N is mainly present as −NH− and $-NH_2$-, mainly through ion complex adsorption of Cr(VI). In this work, FT-IR characterization is used to compare 3D-PCM before and after adsorption (Fig. S5). It was found that the stretching vibration of −OH changed near 3418 cm^{-1}, which confirmed that there was a specific hydrogen bond between −OH and −COOH and Cr(VI). In addition, the $-NH_2$ near 630 cm^{-1} and the C−N group near 1150 cm^{-1} also changed, which indicated that the N-containing functional group was the active adsorption site in the material, which also confirmed the above analysis of Zeta potential. Therefore, the main adsorption mechanisms of Cr(VI) in 3D-PCM include electrostatic interaction, ion complexation,

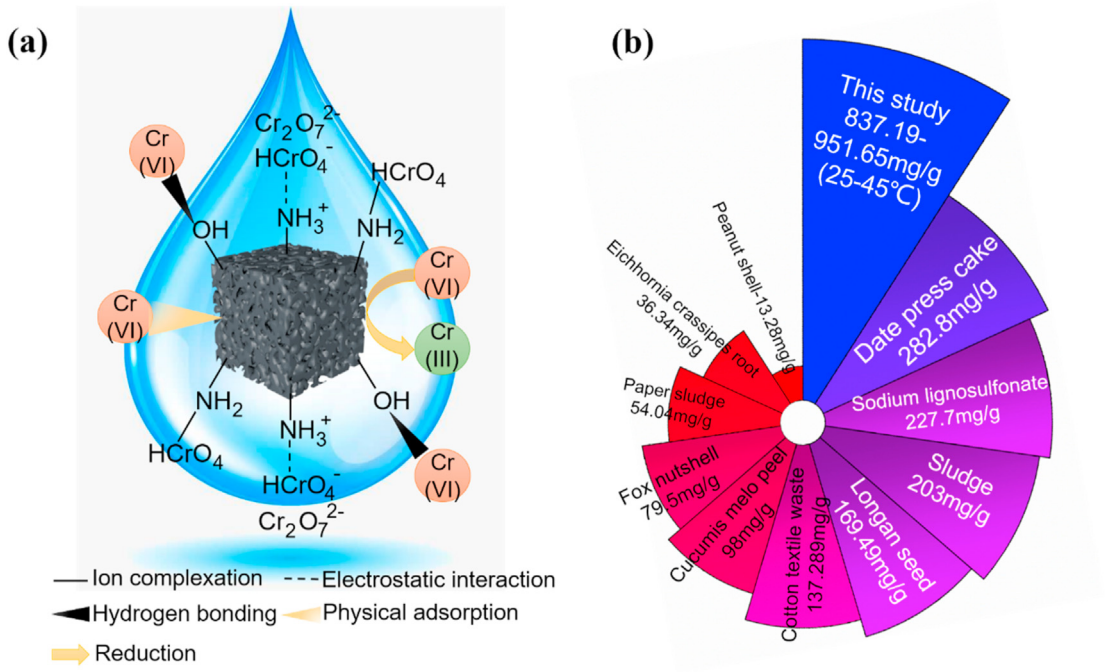

Fig. 10. Schematic illustration of adsorption mechanism(a) and performance comparison(b).

physical adsorption, reduction of Cr(VI) to Cr(III) and hydrogen bonding. A 3D-PCM adsorption mechanism of Cr(VI) is shown in Fig. 10a. In this work, the 3D-PCM maximum adsorption of Cr(VI) on 3D-PCM was 837.19–951.65 mg/g, which is considerably higher than those of similar adsorbents (Fig. 10b and Table S2). The adsorption capacity of Cr(VI) by most of the adsorbents is less than 300 mg/g, which is not conducive to the treatment of high-concentration chromium containing wastewater. However, in real life, the concentration of Cr(VI) in most industrial wastewater is extremely high. Therefore, the adsorption capacity of 3D-PCM as high as 837.19–951.65 mg/g is suitable for actual industrial wastewater treatment, so as to reduce the harm of Cr(VI) brought by the discharge of wastewater into the environment and reduce the negative impact of industrial production.

4. Conclusion

In this work, a novel 3D-PCM was synthesized using glucose and urea by two-stage-hydrothermal and activation method for removal of Cr(VI). The preparation process is simple, green and sustainable. Batch adsorption experiments showed that the 3D-PCM has a high pH dependence on the adsorption of Cr(VI). The Cr(VI) adsorption process on 3D-PCM follows pseudo-second-order kinetics and the Freundlich model, and the adsorption is a spontaneous endothermic reaction, the temperature promotes the adsorption. The maximum adsorption of Cr(VI) on 3D-PCM was 837.19–951.65 mg/g (25–45 °C), which is higher than those of similar adsorbents in the world. The main adsorption mechanisms of Cr(VI) on 3D-PCM include electrostatic interaction, ion complexation, physical adsorption, reduction and hydrogen bonding. The selectivity of 3D-PCM to Cr(VI) was very high in the multivariate ion competition system, which breaks through the problem that most porous carbons are difficult to selectively adsorb Cr(VI). After seven adsorption-desorption cycles, the adsorption performance still has more than 87% of the initial adsorption capacity, which indicated the regeneration performance of 3D-PCM was excellent. Economic cost analysis shows that 3D-PCM has the potential to large-scale production. Therefore, this study provides a new method for synthesizing a novel 3D-PCM, and it can efficiently and selectively remove Cr(VI) from wastewater, which has high application value and is expected to solve the problem of Cr(VI) pollution in water.

CRediT authorship contribution statement

Hongxu Liang: Conceptualization, Methodology, Software, Investigation, Data curation, Writing – original draft. **Hongwei Zhang:** Validation, Formal analysis, Software. **Pinye Zhao:** Validation, Visualization. **Xinkun Zhao:** Resources. **Haowei Sun:** Data curation. **Zengchao Geng:** Resources, Writing – review & editing, Validation, Supervision. **Diao She:** Resources, Writing – review & editing, Supervision, Validation, Project administration.

Declaration of competing interest

The authors declare that they have no known competing financial interests or personal relationships that could have appeared to influence the work reported in this paper.

Acknowledgments

This work was supported by the National Natural Science Foundation of China (31772390), Agricultural Ecological Environment Protection Project of Ministry of Agriculture and Rural Affairs of the People's Republic of China (K3120217004); STS (Science and Technology Service Network Initiative) Program (KFJ-STS-QYZD-177), and West Light Foundation (XAB2018A05) of the Chinese Academy of Science.

Appendix A. Supplementary data

Supplementary data to this article can be found online at https://doi.org/10.1016/j.jclepro.2021.127204.

References

Awual, M.R., 2015. A novel facial composite adsorbent for enhanced copper(II) detection and removal from wastewater. Chem. Eng. J. 266, 368–375.

Awual, M.R., Hasan, M.M., 2015. Fine-tuning mesoporous adsorbent for simultaneous ultra-trace palladium(II) detection, separation and recovery. J. Ind. Eng. Chem. 21, 507–515.

Awual, M.R., 2016. Assessing of lead(II) capturing from contaminated wastewater using ligand doped conjugate adsorbent. Chem. Eng. J. 289, 65–73.

Awual, M.R., 2016a. Solid phase sensitive palladium(II) ions detection and recovery using ligand based effificient conjugate nanomaterials. Chem. Eng. J. 300, 264–272.

Awual, M.R., 2016b. Ring size dependent crown ether based mesoporous adsorbent for high cesium adsorption from wastewater. Chem. Eng. J. 303, 539–546.

Awual, M.R., Hasan, M.M., Khaleque, M.A., Shiekh, M.S., 2016. Treatment of copper(II) containing wastewater by a newly developed ligand based facial conjugate materials. Chem. Eng. J. 288, 368–376.

Awual, M.R., 2017b. New type mesoporous conjugate material for selective optical copper(II) ions monitoring & removal from polluted waters. Chem. Eng. J. 307, 85–94.

Awual, M.R., 2017a. Novel nanocomposite materials for effificient and selective mercury ions capturing from wastewater. Chem. Eng. J. 307, 456–465.

Awual, M.R., 2019b. Effificient phosphate removal from water for controlling eutrophication using novel composite adsorbent. J. Clean. Prod. 228, 1311–1319.

Awual, M.R., 2019a. An effificient composite material for selective lead(II) monitoring and removal from wastewater. J. Environ. Chem. Eng. 7, 103087 https://doi.org/10.1016/j.jece.2019.103087.

Awual, M.R., Hasan, M.M., Asiri, A.M., Rahman, M.M., 2019a. Novel optical composite material for effificient vanadium(III) capturing from wastewater. J. Mol. Liq. 283, 704–712.

Awual, M.R., Hasan, M.M., Rahman, M.M., Asiri, A.M., 2019b. Novel composite material for selective copper(II) detection and removal from aqueous media. J. Mol. Liq. 283, 772–780.

Awual, M.R., Hasan, M.M., Islam, A., Rahman, M.M., Asiri, A.M., Khaleque, M.A., Sheikh, M.C., 2019c. Offering an innovative composited material for effective lead(II) monitoring and removal from polluted water. J. Clean. Prod. 231, 214–223.

Awual, M.R., Hasan, M.M., Asiri, A.M., Rahman, M.M., 2019d. Cleaning the arsenic(V) contaminated water for safe-guarding the public health using novel composite material. Compos. B Eng. 171, 294–301.

Ballav, N., Choi, H.J., Mishra, S.B., Maity, A., 2014. Polypyrrole-coated halloysite nanotube clay nanocomposite: synthesis, characterization and Cr(VI) adsorption behaviour. Appl. Clay Sci. 102, 60–70.

Bhaumik, M., Agarwal, S., Gupta, V.K., Maity, A., 2016. Enhanced removal of Cr(VI) from aqueous solutions using polypyrrole wrapped oxidized MWCNTs nanocomposites adsorbent. J. Colloid Interface Sci. 470, 257–267.

Ding, Z., Liang, J., Zhang, W., Wang, W., Geng, R., Wang, Y., Li, P., Fan, Q., 2020. Efficiency and active sites of the synergetic sorption and photocatalysis in Cr(VI) decontamination on a 3D oxidized graphene ribbon framework. J. Mater. Chem. A Mater. Energy Sustain. 8, 11362–11369.

Gu, H.B., Rapole, S.B., Huang, Y.D., Cao, D.M., Luo, Z.P., Wei, S.Y., Guo, Z.H., 2013. Synergistic interactions between multi-walled carbon nanotubes and toxic hexavalent chromium. J. Mater. Chem. A Mater. Energy Sustain. 1, 2011–2021.

Ho, Y.S., Ng, J.C.Y., McKay, G., 2000. Kinetics of pollutant sorption by biosorbents. Separ. Purif. Methods 29, 189–232.

Kera, N.H., Bhaumik, M., Ballav, N., Pillay, K., Ray, S.S., Maity, A., 2016. Selective removal of Cr(VI) from aqueous solution by polypyrrole/2,5-diaminobenzene sulfonic acid composite. J. Colloid Interface Sci. 476, 144–157.

Ketelle, B.H., Boyd, G.E., 1947. The exchange adsorption of ions from aqueous solutions by organic zeolites. IV. The separation of the yttrium group rare earths1. J. Am. Chem. Soc. 69, 2800–2812.

Ko, Y.J., Choi, K., Lee, S., Jung, K.W., Lee, W.S., 2018. Strong chromate-adsorbent based on pyrrolic nitrogen structure: an experimental and theoretical study on the adsorption mechanism. Water Res. 145, 287–296.

Kumar, A.S.K., Jiang, S.J., Tseng, W.L., 2015. Effective adsorption of chromium (VI)/Cr (III) from aqueous solution using ionic liquid functionalized multiwalled carbon nanotubes as a super sorbent. J. Mater. Chem. A Mater. Energy Sustain. 3, 7044–7057.

Legrouri, K., Khouya, E., Hannache, H., El Hartti, M., Ezzine, M., Naslain, R., 2017a. Activated carbon from molasses efficiency for Cr (VI), Pb (II) and Cu (II) adsorption: a mechanistic study. Chem. Int. 3, 301–310.

Leite, A.J.B., Lima, E.C., dos Reis, G.S., Thue, P.S., Saucier, C., Rodembusch, F.S., Dias, S.L.P., Umpierres, C.S., Dott, G.L., 2017b. Hybrid adsorbents of tannin and APTES (3-aminopropyltriethoxysilane) and their application for the highly efficient removal of acid red 1 dye from aqueous solutions. J. Environ. Chem. Eng. 5, 4307–4318.

Li, L., Feng, X., Han, R., Zang, S., Yang, G., 2017. Cr(VI) removal via anion exchange on a silver-triazolate MOF. J. Hazard Mater. 321, 622–628.

Liang, H.X., Song, B., Peng, P., Jiao, G.J., Yan, X., She, D., 2019. Preparation of three-dimensional honeycomb carbon materials and their adsorption of Cr(VI). Chem. Eng. J. 367, 9–16.

Liang, H.X., Sun, R.R., Song, B., Sun, Q.Q., Peng, P., She, D., 2020. Preparation of nitrogen-doped porous carbon material by a hydrothermal-activation two-step method and its high-efficiency adsorption of Cr(VI). J. Hazard Mater. 387, 121987.

Lima, E.C., Adebayo, M.A., Machado, F.M., 2015. Kinetic and equilibrium models of adsorption. In: Bergmann, C.P., Machado, F.M. (Eds.), Carbon Nanomaterials as Adsorbents for Environmental and Biological Applications. Springer, pp. 33–69.

Lima, E.C., Hosseini-Bandegharaei, A., Moreno-Piraján, J.C., Anastopoulos, I., 2019a. A critical review of the estimation of the thermodynamic parameters on adsorption equilibria. Wrong use of equilibrium constant in the Van't Hoof equation for calculation of thermodynamic parameters of adsorption. J. Mol. Liq. 273, 425–434.

Lima, E.C., Hosseini-Bandegharaei, A., Anastopoulos, I., 2019b. Response to "some remarks on a critical review of the estimation of the thermodynamic parameters on adsorption equilibria. Wrong use of equilibrium constant in the van't Hoff equation for calculation of thermodynamic parameters of adsorption - journal of Molecular Liquids 273 (2019) 425–434. J. Mol. Liq. 280, 298–300.

Liu, S.W., Wang, X.B., Zhao, H.J., Cai, W.P., 2015. Micro/nano-scaled carbon spheres based on hydrothermal carbonization of agarose. Colloids Surf. A Physicochem. Eng. Asp. 484, 386–393.

Lv, Z., Tan, X., Wang, C., Alsaedi, A., Chen, C., 2019. Metal-organic frameworks-derived 3d yolk shell-like structure ni@carbon as a recyclable catalyst for Cr(VI) reduction. Chem. Eng. J. 389, 123428.

Nameni, M., Moghadam, M.R.A., Arami, M., 2008. Adsorption of hexavalent chromium from aqueous solutions by wheat bran. Int. J. Environ. Sci. Technol. 5, 161–168.

O'Connell, D.W., Birkinshaw, C., O'Dwyer, T.F., 2008. Heavy metal adsorbents prepared from the modification of cellulose: a review. Bioresour. Technol. 99, 6709–6724.

Okpalugo, T.I.T., Papakonstantinou, P., Murphy, H., McLaughlin, J., Brown, N.M.D., 2005. High resolution XPS characterization of chemical functionalised MWCNTs and SWCNTs. Carbon 43, 153–161.

Pakade, V.E., Tavengwa, N.T., Madikizela, L.M., 2019. Recent advances in hexavalent chromium removal from aqueous solutions by adsorptive methods. RSC Adv. 9, 26142–26164.

Pan, Z., Zhu, X., Satpathy, A., Li, W., Fortner, J.D., Giammar, D.E., 2019. Cr(VI) adsorption on engineered iron oxide nanoparticles: exploring complexation processes and water chemistry. Environ. Sci. Technol. 53, 11913–11921.

Pradhan, D., Sukla, L.B., Sawyer, M., Rahman, P.K.S.M., 2017. Recentbioreduction of hexavalent chromium in wastewater treatment: a review. J. Ind. Eng. Chem. 55, 1–20.

Ramalingam, B., Parandhaman, T., Choudhary, P., Das, S.K., 2018. Biomaterial functionalized graphene-magnetite nanocomposite: a novel approach for simultaneous removal of anionic dyes and heavy-metal ions. ACS Sustain. Chem. Eng. 6, 6328–6341.

Sun, X., Li, Y., 2004. Colloidal carbon spheres and their core/shell structures with noblemetal nanoparticles. Angew. Chem. 116, 607–611.

Wang, Y., Yu, F., Zhu, M., Ma, C., Zhao, D., Wang, C., Zhou, A., Dai, B., Ji, J., Guo, X., 2018. N-Doping of plasma exfoliated graphene oxide via dielectric barrier discharge plasma treatment for the oxygen reduction reaction. J. Mater. Chem. A Mater. Energy Sustain. 6, 2011–2017.

Wang, Y., Zhao, D., Feng, S., Chen, Y., Xie, R., 2020. Ammonium thiocyanate functionalized graphene oxide-supported nanoscale zero-valent iron for adsorption and reduction of Cr(VI). J. Colloid Interface Sci. 580, 345–353.

Wu, Y., Luo, H.J., Wang, H., Wang, C., Zhang, J., Zhang, Z.L., 2013. Adsorption of hexavalent chromium from aqueous solutions by graphene modified with cetyltrimethylammonium bromide. J. Colloid Interface Sci. 394, 183–191.

Xu, J., Xu, D., Zhu, B., Cheng, B., Jiang, C., 2018. Adsorptive removal of an anionic dye Congo red by flower-like hierarchical magnesium oxide (MgO)-graphene oxide composite microspheres. Appl. Surf. Sci. 435, 1136–1142.

Xu, Y., Chen, J., Chen, R., Yu, P., Guo, S., Wang, X., 2019. Adsorption and reduction of chromium (VI) from aqueous solution using polypyrrole/calcium rectorite composite adsorbent. Water Res. 160, 148–157.

Yang, X., Liu, L., Zhang, M., Tan, W., Qiu, G., Zheng, L., 2019. Improved removal capacity of magnetite for Cr(VI) by electrochemical reduction. J. Hazard Mater. 374, 26–34.

Yuan, D.S., Chen, J.X., Zeng, J.H., Tan, S.X., 2008. Preparation of monodisperse carbon nanospheres for electrochemical capacitors. Electrochem. Commun. 10, 1067–1070.

Zehhaf, A., Benyoucef, A., Quijada, C., Taleb, S., Morallon, E., 2015. Algerian natural montmorillonites for arsenic(III) removal in aqueous solution. Int. J. Environ. Sci. Technol. 12, 595–602.

Zhitkovich, A., 2005. Importance of chromium–DNA adducts in mutagenicity and toxicity of chromium (VI). Chem. Res. Toxicol. 18, 3–11.

Zhu, K., Chen, C., Lu, S., Zhang, X., Alsaedi, A., Hayat, T., 2019. Mofs-induced encapsulation of ultrafine ni nanoparticles into 3d n-doped graphene-cnt frameworks as a recyclable catalyst for Cr(VI) reduction with formic acid. Carbon 148, 52–63.